

Combined impact of strain and stoichiometry on the structural and ferroelectric properties of epitaxially grown $\text{Na}_{1+x}\text{NbO}_{3+\delta}$ films on (110) NdGaO_3

Biya Cai,¹ J. Schwarzkopf,² C. Feldt,² J. Sellmann,² T. Markurt,² and R. Wördenweber^{1,*}

¹*Peter Grünberg Institute (PGI) and JARA-Fundamentals of Future Information Technology, Forschungszentrum Jülich, 52425 Jülich, Germany*

²*Leibniz Institute for Crystal Growth, Max-Born-Strasse 2, 12489 Berlin, Germany*

(Received 7 November 2016; revised manuscript received 2 March 2017; published 23 May 2017)

We demonstrate that the strain of an epitaxially grown film, which is induced by the lattice mismatch between the crystalline substrate and film and relaxes with increasing film thickness, can be conserved beyond the critical thickness of plastic relaxation of the respective film/substrate heterostructure system by adding epitaxially embedded nanoprecipitates and/or nanopillars of a secondary phase. By doing so we modify the ferroelectric properties of the film in a very controlled way. For this purpose, strained $\text{Na}_{1+x}\text{NbO}_{3+\delta}$ films are epitaxially grown on (110) NdGaO_3 and their structural and electronic properties are investigated. X-ray diffraction and transmission electron microscopy analysis indicate that in addition to the epitaxially grown majority phase NaNbO_3 , a second phase $\text{Na}_y\text{NbO}_{3+\delta}$ is present in the films and forms crystalline precipitates and vertically aligned pillars a few nanometers in diameter. For large enough concentrations, this secondary phase appears to be able to suppress the plastic relaxation of the NaNbO_3 matrix. In contrast to stoichiometric films and films with small Na excess, which demonstrate strain relaxation for film thickness exceeding a few nanometers and relaxor-type ferroelectric behavior, the $\text{Na}_{1+x}\text{NbO}_{3+\delta}$ film with the largest off-stoichiometry (grown from a target with $x = 17\%$) exhibits the “classic” ferroelectric behavior of unstrained NaNbO_3 with a hysteretic structural and ferroelectric transition. However, the temperature of this hysteretic transition is shifted from 616 K to 655 K for unstrained material to room temperature for the strained $\text{Na}_{1+x}\text{NbO}_{3+\delta}$ film grown from the off-stoichiometric target.

DOI: [10.1103/PhysRevB.95.184108](https://doi.org/10.1103/PhysRevB.95.184108)

I. INTRODUCTION

Since the discovery of ferroelectricity in 1920, a large number of ferroelectric materials ranging from hydrogen-bonded crystals to double oxides (e.g., titanate or niobate) were identified that show extraordinary dielectric, pyroelectric, elastolectric, or optoelectric properties and, therefore, are of interest for technical applications [1]. Especially in thin-film form, double-oxide ferroelectrics and, more generally, polar materials are today used in memories, sensors, actuators, and RF devices [2]. However, these ferroelectrics typically exhibit most of their profound features in a temperature regime close to the phase transition temperature from the dielectric to the ferroelectric state. In this temperature regime, for instance, the largest permittivity, piezoelectric effect, and tunability are present. Unfortunately, this transition temperature T_C is usually a long way off room temperature, e.g., $T_C \approx 37$ K for SrTiO_3 [3], 403 K for BaTiO_3 [4], 503–760 K (depending on the composition) for $\text{PbZr}_{1-x}\text{Ti}_x\text{O}_3$ [5], 763 K for PbTiO_3 [6], and 628 K for NaNbO_3 [7,8], respectively. Therefore, it is of great interest to modify the phase transition temperature.

This “engineering” of T_C can be achieved via strain, doping, or a combination of both. Especially for epitaxial ferroelectric films, the application of strain has proven to be very successful. Due to the lattice mismatch between the substrate and epitaxially grown film, a tensile or compressive strain is induced at the film-substrate interface (see Fig. 1) and leads to an elastic deformation of the film’s lattice. As a result of this deformation, the ferroelectric properties of these films are modified. This has been demonstrated

for a number of epitaxially grown thin films of perovskite ferroelectrics [9–16], tungsten bronzes [17], and bismuth-layer-structured ferroelectrics [18].

However, at the same time, the strain induced at the film-substrate interface leads to the formation of defects (e.g., dislocations) in the growing film which (i) result in a relaxation of the elastic deformation of the film with increasing film thickness [19] and (ii) tend to cause a slight deviation from the perfect stoichiometry of the film. As a consequence, these ferroelectric films typically show a broad ferroelectric phase transition and a frequency dispersion, which are characteristics of relaxor-type ferroelectric behaviors [11–14]. In order to avoid these effects, the relaxation of the strain in the films must be prevented. A possible way to achieve this is by introducing a secondary phase with a different lattice parameter. If this secondary phase is epitaxially embedded in the primary phase and possesses an adequate lattice parameter, it can preserve the strain and thus avoid the plastic relaxation of the elastically deformed film lattice. Possible solutions to stabilize the strain of the film are illustrated in Fig. 1. These are, for instance, vertically (i.e., out-of-plane) aligned nanocomposites of a secondary phase that grow in the form of pillars normal to the substrate surface [20] [Fig. 1(b)] or nanoprecipitates [Fig. 1(c)] of a secondary phase.

In this report we demonstrate that the conservation of the strain in ferroelectric NaNbO_3 films can be achieved by adding Na during the epitaxial growth. For this purpose, NaNbO_3 with additional Na are epitaxially grown on (110) NdGaO_3 substrates. We demonstrate that in addition to NaNbO_3 , a second phase $\text{Na}_y\text{NbO}_{3+\delta}$ develops in the films if the Na content is large enough. This secondary phase appears to form nanoprecipitates as well as vertically aligned nanopillars, and stabilizes the strain, elastic deformation, and stoichiometry

*Corresponding author: r.woerdenweber@fz-juelich.de

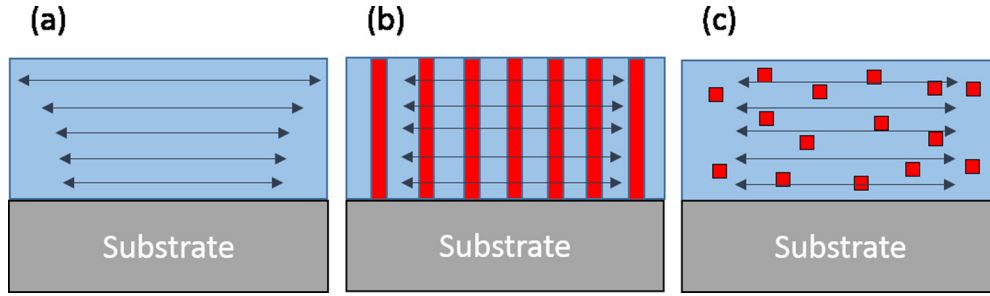


FIG. 1. Sketches of the different concepts of strain engineering of thin epitaxial films for the case of compressive in-plane strain: (a) due to the lattice mismatch between substrate and film, in-plane strain is introduced at the substrate-film interface and leads to an elastic deformation of the film's lattice, which relaxes (due to defects) with the increasing thickness of the film [19]; (b) similarly to (a), however, the elastic deformation is preserved by vertically aligned nanopillars of a secondary phase [20]; and (c) similarly to (a), however, the elastic deformation is preserved by nanoprecipitates of a secondary phase. The arrows indicate the amount of elastic deformation (strain) of the film, and the different colors characterize the different phases, i.e., primary phase (blue) and secondary phase (red).

in the film. In contrast to the nominally stoichiometric NaNbO_3 films, which demonstrate relaxor-type behavior [12–14], these samples exhibit “classic” ferroelectric behavior with the characteristic thermal hysteresis of the permittivity and structural properties upon thermal cycling, albeit at a much lower temperature than their unstrained counterpart due to the compressive in-plane strain.

II. EXPERIMENTAL TECHNIQUES AND SAMPLE PREPARATION

$\text{Na}_{1+x}\text{NbO}_{3+\delta}$ films were deposited by pulsed laser deposition (PLD) on (110) NdGaO_3 substrates using self-made stoichiometric and nonstoichiometric sodium excess targets with a nominal Na/Nb ratio x ranging from 1 to 1.37 in the raw material mixture. The targets are prepared by conventional solid-state reaction. Sodium carbonate (Na_2CO_3 , 99.997% purity) and niobium oxide (Nb_2O_5 , 99.9985% purity) powders are mixed, milled, and pressed into pellets of 2.5 cm in diameter at 2000 bar. Subsequently, the pellets are first calcined for 6 h and in a second step sintered for 12 h at 950 °C inside a Pt/Au crucible in ambient air. The resulting Na/Nb ratio of the sintered target is obtained from inductively coupled plasma optical emission spectroscopy (ICP-OES) with an accuracy of $\Delta x \approx \pm 0.01$. For instance, for a Na/Nb ratio of 1.22 in the raw material mixture, we obtain a Na/Nb ratio of 1.17 ± 0.01 in the target. The Na/Nb ratio in the deposited $\text{Na}_{1+x}\text{NbO}_{3+\delta}$ film is analyzed via energy-dispersive x ray with an accuracy of $\Delta x \approx \pm 0.05$. It agrees quite well with the composition of the target.

For the PLD process, a KrF excimer laser ($\lambda = 248$ nm) with an energy fluence of 2.2 J/cm^2 and a pulse repetition rate of 5 Hz is used. The oxygen pressure during deposition is adjusted to 70 Pa at a substrate temperature of 600 °C. Before deposition, the (110)-oriented single-crystalline NdGaO_3 substrates are annealed in pure oxygen flow at 1050 °C for 1 h. This generates a regular step-and-terrace surface structure with NdO surface termination [21] and promotes step-flow growth of the NaNbO_3 film. The typical thickness of the films described in this report is about 30 nm. More details on the deposition conditions are stated in Ref. [22].

The structural properties of the target and film are analyzed via x-ray diffraction (XRD) and transmission electron microscopy (TEM). The crystallographic phases of the

ceramic targets are determined via standard powder XRD with Cu $K\alpha$ radiation ($\lambda = 1.541 \text{ \AA}$). The structural properties of the NaNbO_3 films are analyzed via high-resolution x-ray diffraction (HRXRD) by a Bruker D8 Discovery with the Cu $K\alpha_1$ line ($\lambda = 1.54056 \text{ \AA}$). Symmetrical θ - 2θ scans are used to determine the out-of-plane lattice parameters of the films and to evaluate the film thickness. Furthermore, two-dimensional (2D) reciprocal space mappings (RSMs) in the vicinity of selected asymmetrical substrate Bragg reflections are recorded in order to investigate the strain state of the films. Orthorhombic (index “o”) and pseudocubic (index “pc”) notations are used for the description of the substrate and film contributions, respectively.

TEM investigations are performed with an FEI Titan 80–300 electron microscope operated at 300 kV. Scanning transmission electron microscopy (STEM) Z-contrast imaging is carried out using a semiconvergence angle of 9.0 mrad for the electron probe (giving a spatial resolution of approximately 1.3 Å) and a semiacceptance angle of the annular dark-field detector (Fishione model 3000) of 35 mrad. Samples for TEM measurements are prepared by mechanical polishing and Ar ion beam milling using a Gatan PIPS with successively decreasing acceleration voltages between 3.5 and 0.2 kV and liquid nitrogen cooling of the sample.

For the investigation of the in-plane dielectric properties of the $\text{Na}_{1+x}\text{NbO}_{3+\delta}$ films, planar capacitors based on interdigitated electrodes (IDEs) are employed. The IDEs are prepared via lift-off lithography technique and deposition of a thin (30-nm) Pt layer [11]. As we do not consider the anisotropy of the lattice strain of the two orthogonal in-plane directions (for this see Ref. [13]) in this work, only IDEs for the electric field oriented along the crystallographic direction with the larger lattice parameter of the substrate are considered, i.e., $E \parallel [-110]\text{NdGaO}_3$. The ferroelectric properties are analyzed as a function of temperature (20 K to 500 K), frequency (20 Hz to 2 MHz), and ac electric field (0.2 V to 5 V). The permittivity ϵ' (real part of the dielectric constant) of the $\text{Na}_{1+x}\text{NbO}_{3+\delta}$ films is calculated using the partial capacitance model [23–25].

III. EXPERIMENTAL RESULTS AND DISCUSSION

XRD powder measurements of the self-made $\text{Na}_{1+x}\text{NbO}_{3+\delta}$ targets with a Na/Nb ratio x ranging from 0 to 0.37 are presented in Fig. 2(a). For targets

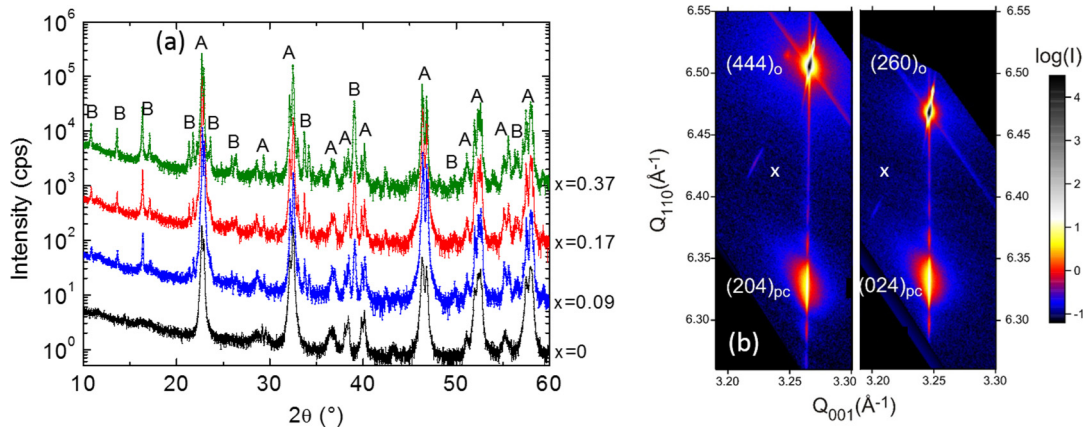


FIG. 2. (a) Powder XRD measurements of $\text{Na}_{1+x}\text{NbO}_{3+\delta}$ targets prepared with Na excess compared to the stoichiometric NaNbO_3 ($x = 0$) composition (see also Supplemental Material). For better visibility the signals are shifted by a factor of 10 for each successive composition; the compositions (x) are given in the figure. Reflection peaks indicated by “A” and “B” are attributed to the NaNbO_3 phase and the Na_3NbO_4 secondary phase, respectively. (b) RSM in the vicinity of the $(444)_o$ and $(260)_o$ Bragg reflections of the NdGaO_3 substrate demonstrate the epitaxial growth of the NaNbO_3 phase for the $\text{Na}_{1.17}\text{NbO}_{3+\delta}$ film on NdGaO_3 , the white crosses marking the position of unstrained NaNbO_3 .

which are prepared with Na excess ($x > 0$) compared to the stoichiometric NaNbO_3 target ($x = 0$), we observe the occurrence of an extra phase (labeled as “B”) in addition to the main perovskite NaNbO_3 phase [marked as “A” in Fig. 2(a)]. From a detailed analysis of the powder XRD data (see also Supplemental Material [26]) we identify phase “B” to be Na_3NbO_4 (01-070-2005), which exhibits a monoclinic structure with lattice parameters of $a = 11.126 \text{ \AA}$, $b = 12.988 \text{ \AA}$, $c = 5.746 \text{ \AA}$, and $\beta = 109.4^\circ$ [27]. The appearance of the Na_3NbO_4 phase for Na-rich conditions is in agreement with the $\text{Na}_2\text{O-Nb}_2\text{O}_5$ phase diagram [27]. Although the intensities of the peaks of the extra phases increase with a rising amount of Na excess, they are small compared to the reflected intensity of the NaNbO_3 phase. This indicates that NaNbO_3 still represents the main phase in the nonstoichiometric targets. For convenience we will denote the targets by their nominal composition x using $\text{Na}_{1+x}\text{NbO}_{3+\delta}$ in the following.

According to our previous work [12–14], stoichiometric NaNbO_3 films grow on $(110)\text{NdGaO}_3$ substrates with a $(001)_{pc}$ surface orientation and in-plane epitaxial orientation $[010]_{pc} \parallel [-110]_o$ and $[100]_{pc} \parallel [001]_o$ (for more information see Supplemental Material [26]). This is also the case for the growth of NaNbO_3 from nonstoichiometric targets, which is demonstrated by RSMs recorded in the vicinity of the asymmetric $(444)_o$ and $(260)_o$ Bragg reflections of the orthorhombic NdGaO_3 substrate [see Fig. 2(b)]. The RSM patterns prove the epitaxial, pseudomorphic growth of the films grown from targets with Na excess on the NdGaO_3 substrate, as the in-plane components of the scattering vectors of the NdGaO_3 substrate and of the main intensity of the corresponding Bragg reflection of the NaNbO_3 film coincide.

High-resolution XRD scans (see Supplemental Material [26]) recorded between $2\theta = 10^\circ$ and 60° exhibit only Bragg reflection peaks of the $(110)_o$ -oriented NdGaO_3 substrate and of the $(001)_{pc}$ -oriented NaNbO_3 film for all samples, including those grown from targets with excess Na. No foreign phase could be detected in these measurements. The reason for this might be simply that the additional

phase forms small clusters which are too small for detection via XRD.

High-resolution Bragg-Brentano diffraction curves measured in the vicinity of the Bragg reflection peaks of the NdGaO_3 substrate are shown in Fig. 3(a). In contrast to the diffractogram of the NaNbO_3 film grown from the stoichiometric target, the film grown from the Na excess target shows pronounced thickness oscillations, proving a smooth surface and interface. From the angular position of the Bragg peak of the reference film (stoichiometric target) at about $2\theta = 46.245^\circ$, a vertical lattice spacing of the epitaxial NaNbO_3 phase of $d_\perp = 3.923 \text{ \AA}$ can be deduced for room temperature. Heating and cooling of the sample leads to a reversible, linear, small increase of the lattice parameter with increasing temperature [Fig. 3(b)]. The lattice parameter is only slightly larger than the lattice parameter of unstrained bulk material [dashed-dotted line in Fig. 3(b)], indicating that the initial strain of the film is strongly relaxed.

However, the film grown from the off-stoichiometric target $\text{Na}_{1+x}\text{NbO}_{3+\delta}$ with $x = 0.17$ behaves differently. (For convenience the resulting film is denoted $\text{Na}_{1.17}\text{NbO}_{3+\delta}$, in accordance with its nominal stoichiometry in the following; see also Supplemental Material [26].) It exhibits:

- (i) a larger lattice spacing d_\perp , which is attributed to a larger effective in-plane compressive strain (i.e., less relaxation of the elastic deformation of the film),
- (ii) a stronger temperature dependence of d_\perp compared to that of the reference sample, and
- (iii) a hysteretic change of the lattice parameter upon thermal cycling [Fig. 3(b)]. This hysteretic behavior is reproducible upon multiple thermal cycles.

Whereas the first observation indicates that plastic relaxation of the strain of the NaNbO_3 films is suppressed by the growth from a nonstoichiometric target, the last observation points to a hysteretic structural transition of the film material. Figure 3(c) indicates that the behavior actually changes around a Na excess in the target of about $x \approx 0.075$. Up to $x \approx 0.075$ the lattice parameter is not affected by the additional Na; above $x = 0.1$ the lattice parameter of the NaNbO_3 film

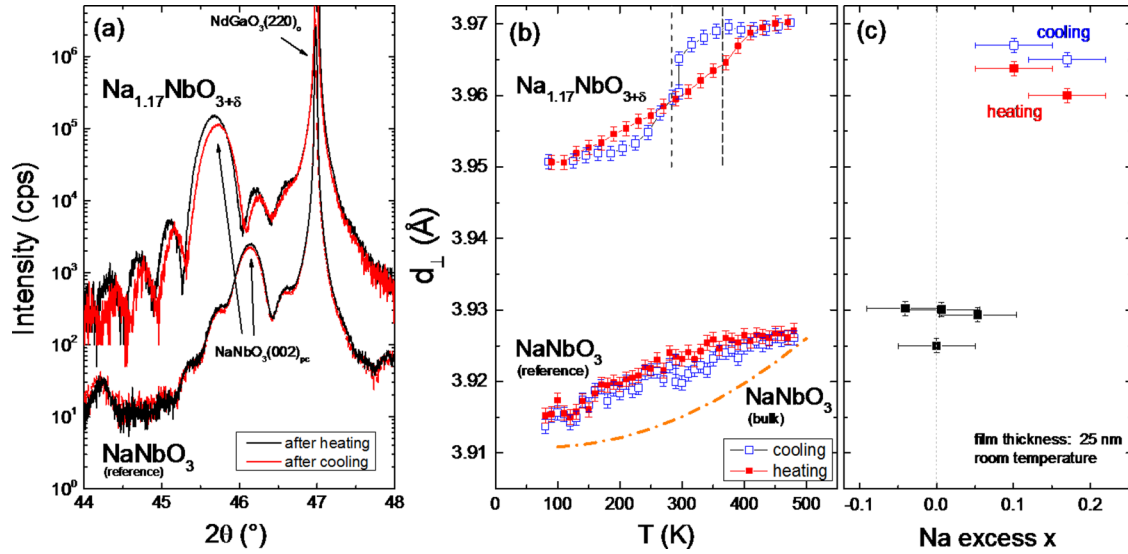


FIG. 3. (a) Magnified HRXRD scans of the reference sample grown from a stoichiometric NaNbO_3 target (lower curves) and a sample grown from a $\text{Na}_{1.17}\text{NbO}_{3+\delta}$ target (upper curves; the intensity is shifted by a factor of 100) recorded at room temperature around the $(220)_c$ reflection peak of the NdGaO_3 substrate after heating to 400 K (black curve) and after cooling to 80 K (red curve). (b) Temperature dependence of the vertical lattice parameter of the NaNbO_3 phase for a reference sample and for the film grown from the $\text{Na}_{1.17}\text{NbO}_{3+\delta}$ target for cooling (open blue symbols) and heating (solid red symbols). The orange dashed-dotted line in (b) represents the simulated out-of-plane lattice parameter for unstrained bulk NaNbO_3 [28]. The dashed lines in (b) mark the temperature of the hysteric ferroelectric phase transition (see Fig. 4). (c) Vertical lattice parameter of the NaNbO_3 phase of epitaxial $\text{Na}_{1+x}\text{NbO}_{3+\delta}$ films on (110) NdGaO_3 grown from targets with Na excess x .

increases abruptly by approximately 1% compared to the case of stoichiometric or lower Na excess samples, and the lattice parameter exhibits additionally a hysteretic behavior upon thermal cycling.

In order to obtain a more detailed insight into the microstructure of the NaNbO_3 film grown from a Na excess target, (S)TEM investigations were performed. Dark-field TEM imaging of the film under $g = 110_{\text{NdGaO}_3}$ two-beam conditions [Fig. 4(a)] reveals the presence of vertically aligned pillars which proceed through the whole film and have a width of typically 2 nm. The spatial distribution of the pillars within the film is rather inhomogeneous on a length scale of several 100 nm; however, their average density is of the order of

10^{10}cm^{-2} . Additionally, we observed nanoprecipitates with a typical diameter of $\sim 5\text{nm}$ in the film [Fig. 4(b)]. Their density in the NaNbO_3 film is close to the detection limit of TEM of about $10^{12} - 10^{13}\text{cm}^{-3}$. Further information about the precipitates can be obtained by analyzing the pattern of the high-resolution STEM Z-contrast images. For their interpretation it has to be considered that the bright intensity maxima in the NaNbO_3 film correspond to heavy Nb atomic columns ($Z = 41$), while Na columns ($Z = 11$) produce only a faint grayish intensity maxima [see Fig. 4(c)], and O columns ($Z = 8$) cannot be seen due to their small atomic number. Comparing the pattern of the NaNbO_3 matrix with that of the precipitate region gives the following results: (i) We do not observe inserted half planes nor a violation of the translation symmetry in the NaNbO_3 matrix across the precipitate. (ii) Within the precipitate region bright intensity maxima are found at positions which correspond to (dark grayish) Na atomic columns in the surrounding matrix [see Fig. 4(c)]. The absolute intensity of the bright maxima in the precipitate region is lower than that of Nb atomic columns in the surrounding NaNbO_3 matrix. However, the mean intensity averaged within the projected perovskite unit cell does not change between the precipitate region and matrix. (iii) The mean intensity of the NaNbO_3 matrix directly surrounding the precipitate (approximately 1 nm rim) has a slightly reduced intensity. This might be related to dechanneling induced by a local lattice distortion rather than by changes in the composition [29].

All results together indicate the presence of a secondary phase, which has a similar symmetry and composition as the NaNbO_3 film. The secondary phase forms precipitates and vertically aligned pillars that grow coherently embedded in the NaNbO_3 matrix but induce a local strain field into the NaNbO_3 matrix.

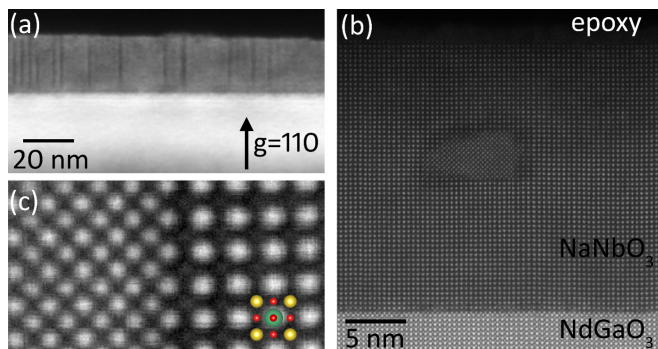


FIG. 4. Cross-sectional (S)TEM images of an epitaxial NaNbO_3 film on a NdGaO_3 substrate grown from a Na excess target: (a) dark-field TEM micrograph recorded under $g = 110_{\text{NdGaO}_3}$ two-beam conditions; (b) STEM Z-contrast image; (c) magnified view from (b) with a model of the pseudocubic unit cell of NaNbO_3 where green, yellow, and red balls represent Nb, Na, and O atoms, respectively.

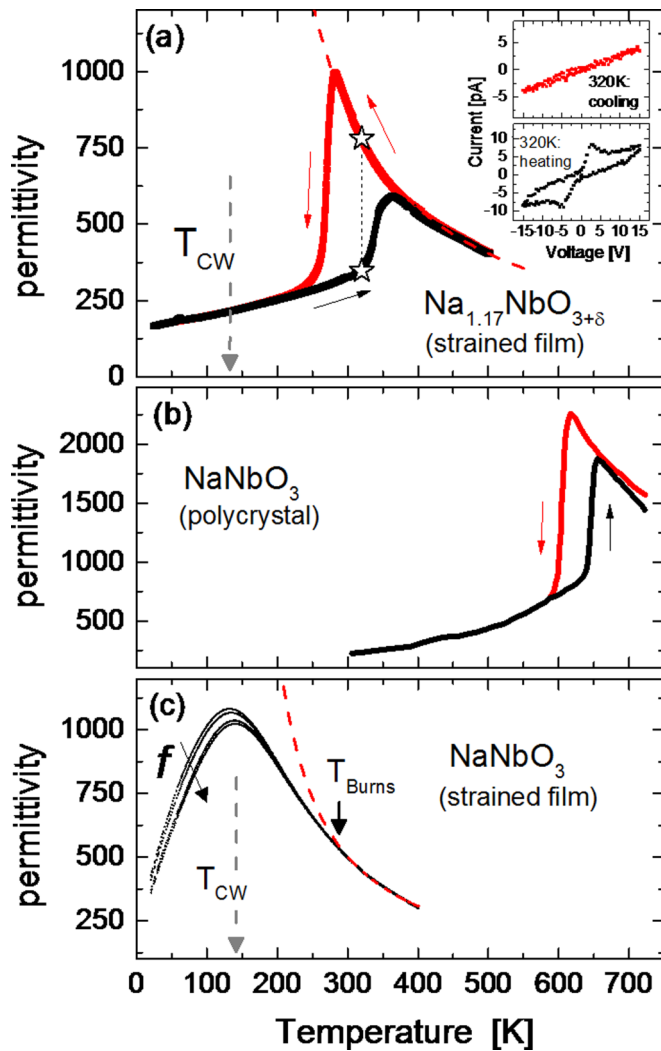


FIG. 5. Comparison of the temperature dependence of (a) the nonstoichiometric film $\text{Na}_{1.17}\text{NbO}_{3+\delta}$ on (110)NdGaO₃, (b) polycrystalline NaNbO_3 (adapted from [8]), and (c) nominally stoichiometric NaNbO_3 on (110)NdGaO₃. The insets in (a) show the current-voltage characteristics for sample $\text{Na}_{1.17}\text{NbO}_{3+\delta}$ recorded at 320 K for cooling (red) and heating (black). The films in (a) and (c) are ~ 27 nm thick; the direction of the thermal cycling in (a) and (b) are indicated by the arrows; the red dashed lines in (a) and (c) show the Curie-Weiss fit with a Curie-Weiss temperature T_{CW} and Burns temperature T_{Burns} . In (c) data sets for different frequencies are given. The frequency increases as indicated by the arrow from 15 kHz (highest permittivity) to 1.5 MHz (lowest permittivity).

The exact nature of the precipitates and vertical pillars, however, could not be unambiguously identified so far. A detailed structural analysis of these defects in NaNbO_3 films grown from nonstoichiometric $\text{Na}_{1+x}\text{NbO}_{3+\delta}$ targets is planned for a forthcoming paper. In this present paper, we will now concentrate on the electronic properties of these films. We will show that a thermal hysteretic behavior is also observed in the ferroelectric properties of the films.

Figure 5 shows a comparison of the temperature dependence of the $\text{Na}_{1.17}\text{NbO}_{3+\delta}$ film [Fig. 5(a)], a typical representative of a nominally stoichiometric NaNbO_3 film

[Fig. 5(c)], and an unstrained NaNbO_3 polycrystalline bulk sample [8] [Fig. 5(b)]. Both films [Figs. 5(a) and 5(c)] are deposited on (110)NdGaO₃, possess a thickness of 27 nm, and are characterized with the electric field oriented along the $[-110]$ NdGaO₃. In contrast to the stoichiometric NaNbO_3 film, the $\text{Na}_{1.17}\text{NbO}_{3+\delta}$ film demonstrates a number of interesting features:

(i) A huge anomalous thermal hysteresis upon cooling and heating is visible around room temperature. This hysteretic behavior is reproducible upon multiple thermal cycles. The peak position in permittivity is shifted by ~ 80 K, and the difference in the permittivity for cooling and heating exceeds 600 at room temperature. The reference film [Fig. 5(c)] exhibits no hysteretic behavior at all. However, the unstrained NaNbO_3 polycrystal does show a quite similar thermal hysteresis but at a much higher temperature (around 620–660 K).

(ii) Both peaks in the permittivity of the $\text{Na}_{1.17}\text{NbO}_{3+\delta}$ film are well defined and sharp, whereas the NaNbO_3 film exhibits a broad peak, which is typical for the phase transition from the dielectric to a relaxor-type ferroelectric state [12–14].

(iii) The $\text{Na}_{1.17}\text{NbO}_{3+\delta}$ film shows no frequency dispersion, which again indicates the absence of relaxor-type behavior in this sample. In contrast, the stoichiometric NaNbO_3 film displays the typical frequency dispersion of a relaxor-type ferroelectric.

First, let us briefly focus on the ferroelectric phase transition and phases of the nonstoichiometric $\text{Na}_{1.17}\text{NbO}_{3+\delta}$ film. Current-voltage characteristics (IVC) present an ideal tool to distinguish between the ferroelectric and the dielectric state. The insets of Fig. 5(a) show IVCs measured at the same temperature, i.e., 320 K, in the regime of the hysteresis for cooling and heating. Upon cooling (upper inset), a linear and nonhysteretic correlation between the current and the voltage indicates that the sample is in the dielectric state, whereas the IVC measured at 320 K upon heating (lower inset) shows a small hysteresis and two peaks, which represent the switching current of the polarization. Thus, within the branches of the hysteresis, the sample seems to be dielectric upon cooling but ferroelectric upon heating. This observation is supported by the Curie-Weiss behavior according to $\epsilon'(T) = C/(T - T_{CW})$, which fits the data obtained at high temperatures (above the peak) for heating and cooling [see Fig. 5(a)]. The values of the Curie constant $C = 1.56 \times 10^5$ K [for the nonstoichiometric film in Fig. 5(a)] and $C = 0.8 \times 10^5$ K (for the stoichiometric film in Fig. 5(c) with a Burns temperature T_{Burns} of ~ 286 K) indicate that both films represent displacement-type ferroelectrics [30]. Also the Curie-Weiss temperatures T_{CW} of the two films are quite similar, ~ 132 K and ~ 140 K for the nonstoichiometric and stoichiometric sample, respectively.

Second, there is the question of whether, similarly to the reference thin film, the ferroelectric state of the nonstoichiometric $\text{Na}_{1.17}\text{NbO}_{3+\delta}$ film represents a relaxor-type ferroelectric state. One indication arguing against a relaxor-type state is the absence of the frequency dispersion that is typically observed in relaxor ferroelectrics during the transition from the dielectric to the ferroelectric state. Another indication is the sharpness of the peak at the transition. For this purpose, the transition

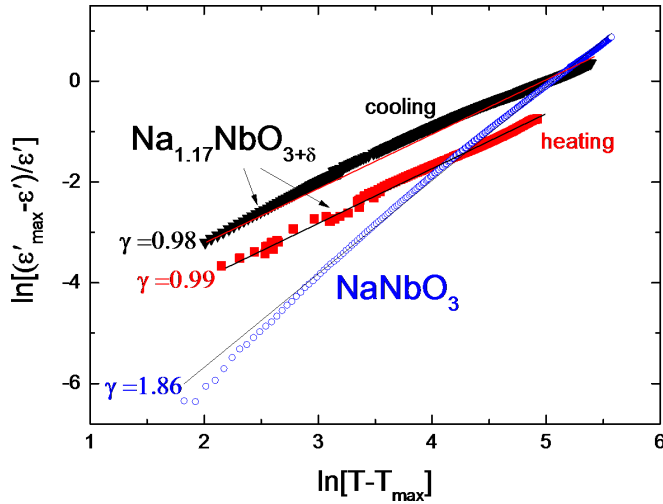


FIG. 6. Lorentz fit of the ferroelectric transition for the stoichiometric NaNbO_3 film (blue open symbols for heating and cooling) and the nonstoichiometric $\text{Na}_{1.17}\text{NbO}_{3+\delta}$ film (red solid squares for heating and black solid triangles for cooling) according to Eq. (1). The solid lines represent the slope γ , the values of γ are given in the figure, and the standard deviation of the fits is smaller than 0.003.

range can be described by a Lorentz simulation [31]:

$$(\varepsilon'_{\max} - 1)/\varepsilon' = (T - T_{\max})^\gamma / 2\sigma^2. \quad (1)$$

Here, ε'_{\max} is the maximum permittivity at T_{\max} , γ is the degree of the dielectric relaxation, and σ is the degree of diffuseness of the phase transition. A classic ferroelectric phase transition is described by $\gamma \approx 1$, whereas values of $\gamma \approx 1.5-2$ are associated with a relaxor-type ferroelectric transition. In contrast to the stoichiometric NaNbO_3 film, which shows a diffuse transition with $\gamma \approx 1.86$, we obtain values of $\gamma \approx 0.99$ on heating and $\gamma \approx 0.98$ on cooling for the $\text{Na}_{1.17}\text{NbO}_{3+\delta}$ film (see Fig. 6). This confirms that in contrast to the stoichiometric film, the nonstoichiometric sample represents a “classic” (i.e., nonrelaxor) ferroelectric system.

Finally, thermal hysteresis has been reported for a few systems. These are, for instance, single crystals of NaNbO_3 [7,32] and BaTiO_3 [33], polycrystalline NaNbO_3 [8], polycrystalline tetragonal tungsten bronze materials [29,34], Langmuir-Blodgett-deposited polymer films [35], or $(\text{PbTiO}_3)_y(\text{BiZn}_{0.5}\text{Ti}_{0.5}\text{O}_3)_{1-y}$ [36], $(\text{NaNbO}_3)_y(\text{SrZrO}_3)_{1-y}$ [37], or $(\text{NaNbO}_3)_x(\text{CaZrO}_3)_{1-x}$ [38] solid solutions.

Generally, there exist three possible explanations for the thermal hysteresis:

- (i) a first-order structural phase transition [7,8,39,40],
- (ii) the presence of two sets of active cation sites in combination with a weak superstructure that changes from an incommensurate to a commensurate structure on cooling [30,34], and
- (iii) a 2D size effect [35].

In our case, we observe a huge difference in T_{\max} and ε'_{\max} between heating and cooling cycles. The size of the hysteresis and the fact that our films are relatively thick compared to the Langmuir-Blodgett layers that showed the 2D size effect allow us to exclude option (iii), i.e., the 2D size effect. Furthermore,

in unstrained NaNbO_3 , a commensurate-to-incommensurate transition is known to occur at a temperature of around 443 K, leading to a featured anomaly [8]. However, this effect is also small and it does not exhibit a thermal history. Therefore, we can also rule out option (ii).

The thermal anomaly in the $\text{Na}_{1.17}\text{NbO}_{3+\delta}$ film shows quite similar features compared to the thermal hysteresis obtained in polycrystalline NaNbO_3 [see Fig. 5(b)]. Moreover, we obtained a hysteretic structural change at the exact temperature where the thermal hysteresis takes place in the permittivity [see Fig. 3(b)]. Therefore, only the first explanation might serve as an explanation in terms of a hysteretic structural transition. For the unstrained polycrystalline NaNbO_3 , there exists a phase transition from the antiferroelectric P phase to the antiferroelectric R phase that takes place at about 616 K for cooling and 655 K for heating. In our case, we measure only one component of the polarization, i.e., the in-plane polarization of an epitaxial film. Therefore, the ferroelectric state might appear differently in these experiments compared to the analysis of the polarization of the polycrystalline sample. Nevertheless, we do see a phase transition (ferroelectric-to-dielectric) which is very similar in appearance to the one observed for stoichiometric polycrystalline material, albeit at a much lower temperature (room temperature) in our strained nonstoichiometric film.

In conclusion of this section, the existing compressive strain seems to successfully reduce the temperature of the hysteresis ferroelectric transition from 616 K (cooling) and 655 K (heating) for the polycrystalline NaNbO_3 to more or less room temperature for the strained nonstoichiometric $\text{Na}_{1.17}\text{NbO}_{3+\delta}$ film. The absence of the relaxor behavior in this sample, which was observed in the strained stoichiometric NaNbO_3 films [12–14], is a clear indication that there is no significant strain relaxation in the case of the nonstoichiometric film. In combination with the RSM [Fig. 2(b)] and XRD [Fig. 3(b)] measurements, we conclude that the $\text{Na}_{1.17}\text{NbO}_{3+\delta}$ film is more homogeneously deformed than the NaNbO_3 thin films with comparable thickness. This might be caused by the stabilizing or buffering effect of the epitaxially embedded precipitates and vertically aligned pillars of the secondary phase $\text{Na}_y\text{NbO}_{3+\delta}$ (see Fig. 4).

IV. CONCLUSIONS

Strained NaNbO_3 thin films are epitaxially grown on (110) NdGaO_3 substrates. TEM measurements show that for NaNbO_3 films grown from nonstoichiometric targets (Na excess), the majority phase NaNbO_3 forms an epitaxially grown matrix with coherently embedded nanometer-sized precipitates and vertically aligned pillars of a secondary phase $\text{Na}_y\text{NbO}_{3+\delta}$. These nanoprecipitates and/or nanopillars seem to be able to suppress the relaxation of the lattice-mismatch-induced strain of the NaNbO_3 matrix which is otherwise observed for stoichiometric NaNbO_3 films on NdGaO_3 with thicknesses exceeding the critical value of typically 10–15 nm [41]. In contrast to NaNbO_3 films grown from stoichiometric targets, which show strain relaxation and a relaxor-type ferroelectric behavior [12–14], the $\text{Na}_{1.17}\text{NbO}_{3+\delta}$ films exhibits the “classic” ferroelectric behavior of unstrained NaNbO_3 with a hysteretic structural and ferroelectric

transition. However, the temperature of this hysteretic transition is shifted from 616 K (cooling) and 655 K (heating) for unstrained bulk material to room temperature, 284 K (cooling) and 364 K (heating), for the strained $\text{Na}_{1.17}\text{NbO}_{3+\delta}$ film.

We believe that our observations illustrate the potential of strain engineering and stoichiometry variation in ferroelectric thin films. For NaNbO_3 we demonstrate that an elastic deformation of an epitaxially grown film induced by the lattice mismatch between film and substrate [here (110) NdGaO_3] is conserved via adequate modification of the stoichiometry. The conservation of the epitaxial strain together via the off-stoichiometry of the NaNbO_3 thin film not only strongly modifies the transition temperature to the ferroelectric state, but also leads to a change of the behavior of the material in the ferroelectric state, ranging from the classic ferroelectric behavior (observed for samples with perfect stoichiometry [16]) and relaxor-type behavior (slightly nonstoichiometric sample due to strain) to again classic ferroelectric behavior for large off-stoichiometry with a secondary phase stabilizing the strain. The question of whether this is a general feature of changing the stoichiometry in complex oxide films or whether it is

unique for the examined system, $\text{Na}_{1+x}\text{NbO}_{3+\delta}$, could be an interesting topic for the future.

Finally, it is not only the possibility of engineering the ferroelectric properties via strain, but also the prominent relaxor properties of the strained NaNbO_3 films and thermal hysteretic behaviors of $\text{Na}_{1.17}\text{NbO}_{3+\delta}$ thin films that represent interesting opportunities for basic research and understanding, as well as possible applications of this type of ferroelectrics. The idea of introducing nonstoichiometry in addition to epitaxial growth opens a new and intriguing possibility for the engineering of a “3D” strain-induced deformation of the lattice.

ACKNOWLEDGMENTS

The authors would like to thank A. Offenhäusser, P.-E. Janolin, M. Schmidbauer, R. Bertram, A. Markov, E. Hollmann, Junmiao Wang, R. Kutzner, S. Trellekamp, and Yang Dai for their valuable support. B.C. would like to thank the China Scholarship Council (CSC) for its financial support under Grant No. 201206400055.

-
- [1] L. E. Cross, *Ferroelectrics* **76**, 241 (1987).
- [2] N. Setter, D. Damjanovic, L. Eng, G. Fox, S. Gevorgian, S. Hong, A. Kingon, H. Kohlstedt, N. Y. Park, G. B. Stephenson *et al.*, *J. Appl. Phys.* **100**, 051606 (2006).
- [3] K. A. Muller, W. Berlinger, and E. Tossati, *Z. Phys. B* **84**, 277 (1991).
- [4] M. B. Smith, K. Page, T. Siegrist, P. L. Redmond, E. C. Walter, R. Seshadri, L. E. Brus, and M. L. Steigerwald, *J. Am. Chem. Soc.* **130**, 6955 (2008).
- [5] B. Jaffe, W. R. Cook, and H. L. Jaffe, *Piezoelectric Ceramics* (Academic Press, London, 1971), p. 135.
- [6] A. M. Glazer and S. A. Mabud, *Acta Crystallogr. B* **34**, 1065 (1978).
- [7] G. Shirane, R. Newnham, and R. Pepinsky, *Phys. Rev.* **96**, 581 (1954).
- [8] H. Guo, H. Shimizu, and C. A. Randall, *Appl. Phys. Lett.* **107**, 112904 (2015).
- [9] J. H. Haeni, P. Irvin, W. Chang, R. Uecker, P. Reiche, Y. L. Li, S. Choudhury, W. Tian, M. E. Hawley, B. Craigo *et al.*, *Nature (London)* **430**, 758 (2004).
- [10] R. Wördenweber, E. Hollmann, R. Kutzner, and J. Schubert, *J. Appl. Phys.* **102**, 044119 (2007).
- [11] R. Wördenweber, J. Schubert, T. Ehlig, and E. Hollmann, *J. Appl. Phys.* **113**, 164103 (2013).
- [12] R. Wördenweber, J. Schwarzkopf, E. Hollmann, A. Duk, B. Cai, and M. Schmidbauer, *Appl. Phys. Lett.* **103**, 132908 (2013).
- [13] B. Cai, J. Schwarzkopf, E. Hollmann, M. Schmidbauer, M. O. Abdel-Hamed, and R. Wördenweber, *J. Appl. Phys.* **115**, 224103 (2014).
- [14] B. Cai, J. Schwarzkopf, E. Hollmann, D. Braun, M. Schmidbauer, T. Grellmann, and R. Wördenweber, *Phys. Rev. B* **93**, 224107 (2016).
- [15] J. F. Ihlefeld, C. M. Folkman, S. H. Baek, G. L. Brennecke, M. C. George, J. F. Carroll III, and C. B. Eom, *Appl. Phys. Lett.* **97**, 262904 (2010).
- [16] C.-H. Lee, V. Skoromets, M. D. Biegalski, S. Lei, R. Haislmaier, M. Bernhagen, R. Uecker, Xiaoxing Xi, V. Gopalan, X. Martí, S. Kamba, P. Kužel, and D.G. Schlom, *Appl. Phys. Lett.* **102**, 082905 (2013).
- [17] A. Infortuna, P. Murali, M. Cantoni, and N. Setter, *J. Appl. Phys.* **100**, 104110 (2006).
- [18] D. Bao, S. K. Lee, X. Zhu, M. Alexe, and D. Hesse, *Appl. Phys. Lett.* **86**, 082906 (2005).
- [19] Y. Dai, J. Schubert, E. Hollmann, G. Mussler, and R. Wördenweber, *J. Appl. Phys.* **120**, 114101 (2016).
- [20] W. Zhang, A. Chen, Z. Bi, Q. Jia, J. L. MacManus-Driscoll, and H. Wang, *Curr. Opin. Solid State Mater. Sci.* **18**, 6 (2014).
- [21] R. Dirsyte, J. Schwarzkopf, G. Wagner, J. Lienemann, M. Busch, H. Winter, and R. Fornari, *Appl. Surf. Sci.* **255**, 8685 (2009).
- [22] J. Sellmann, J. Schwarzkopf, A. Kwasniewski, M. Schmidbauer, D. Braun, and A. Duk, *Thin Solid Films* **570**, 107 (2014).
- [23] O. G. Vendik, S. P. Zubko, and M. A. Nikol'skii, *Tech. Phys.* **44**, 349 (1999); O. G. Vendik and M. A. Nikol'skii, *ibid.* **46**, 112 (2001).
- [24] S. S. Gevorgian, T. Martinsson, P. L. Linner, and E. L. Kollberg, *IEEE Trans. Microwave Theory Technol.* **44**, 896 (1996).
- [25] E. Chen and S. Y. Chou, *IEEE Trans. Microwave Theory Technol.* **45**, 939 (1997).
- [26] See Supplemental Material at <http://link.aps.org/supplemental/10.1103/PhysRevB.95.184108> for information on the structural properties of NaNbO_3 and Na_3NbO_4 , the lattice mismatch between NaNbO_3 and (110) NdGaO_3 , the XRD characterization of the targets with nominal stoichiometry $\text{Na}_{1+x}\text{NbO}_{3+\delta}$, and XRD RSM data of NaNbO_3 films on NdGaO_3 .
- [27] J. Darriet and J. Galy, *Bull. Soc. Fr. Mineral. Cristallogr.* **97**, 3 (1974).
- [28] V. S. Bondarev, A. V. Kartashev, M. V. Gorev, I. N. Flerov, E. I. Pogorel'tsev, M. S. Molokeev, S. I. Raevskaya, D. V. Suzdalev, and I. P. Raevskii, *Phys. Solid State* **55**, 821 (2013).

- [29] V. Grillo, K. Mueller, K. Volz, F. Glas, T. Grieb, and A. Rosenauer, *J. Phys.: Conf. Ser.* **326**, 012006 (2011).
- [30] X. L. Zhu and X. M. Chen, *Appl. Phys. Lett.* **96**, 032901 (2010).
- [31] A. A. Bokov and Z.-G. Ye, *Solid State Commun.* **116**, 105 (2000).
- [32] L. E. Cross and B. J. Nicholson, *Philos. Mag.* **46**, 453 (1955).
- [33] W. J. Merz, *Phys. Rev.* **76**, 1221 (1949).
- [34] M. Prades, H. Beltrán, N. Masó, E. Cordoncillo, and A. R. West, *J. Appl. Phys.* **104**, 104118 (2008).
- [35] A. V. Bune, V. M. Fridkin, S. Ducharme, L. M. Blinov, S. P. Palto, A. V. Sorokin, S. G. Yudin, and A. Zlatkin, *Nature (London)* **391**, 874 (1998).
- [36] M. R. Suchomel and P. K. Davies, *Appl. Phys. Lett.* **86**, 262905 (2005).
- [37] H. Guo, H. Shimizu, Y. Mizuno, and C. A. Randall, *J. Appl. Phys.* **117**, 214103 (2015).
- [38] H. Shimizu, H. Guo, S. E. Reyes-Lillo, Y. Mizuno, K. M. Rabe, and C. A. Randall, *Dalton Trans.* **44**, 10763 (2015).
- [39] A. M. Glazer and H. D. Megaw, *Acta Cryst.* **A29**, 489 (1973).
- [40] S. K. Mishra, R. Mittal, V. Yu. Pomjakushin, and S. L. Chaplot, *Phys. Rev. B* **83**, 134105 (2011).
- [41] J. Schwarzkopf, M. Schmidbauer, T. Remmele, A. Duk, A. Kwasniewski, S. Bin Anooz, A. Devi, and R. Fornari, *J. Appl. Crystallogr.* **45**, 1015 (2012).